RSC Advances

PAPER

View Article Online
View Journal | View Issue

Cite this: *RSC Adv.*, 2017, **7**, 50786

Mechanism of asphaltene aggregation induced by supercritical CO_2: insights from molecular dynamics simulation†

Bing Liu,* Jiawei Li, Chao Qi, Xiaoqi Li, Tingyi Mai and Jun Zhang*

Received 1st September 2017
Accepted 8th October 2017

DOI: 10.1039/c7ra09736k

rsc.li/rsc-advances

The mechanisms of asphaltene aggregation leading to damage and wellbore plugging are still unknown, which is not conducive to finding effective solutions to the relevant problems of asphaltene precipitation in supercritical CO_2 ($scCO_2$) enhanced oil recovery processes. Therefore, molecular dynamics simulations were performed on an oil–$scCO_2$ system to investigate the behavior and mechanism of asphaltene aggregation. The results show that the selective extraction of crude oil in $scCO_2$ leads to the formation of asphaltene nanoaggregates. The vdW interactions among asphaltenes in $scCO_2$ are stronger than those under vacuum, which aggravates aggregation. Free energy calculations indicate that the remaining binding energy between asphaltenes in $scCO_2$ is the driving force of asphaltene aggregation. Interestingly, we observed a two-step process of separation and aggregation for asphaltene nanoaggregates, which demonstrates that the efficiency of inhibiting asphaltene aggregation can be improved by adding an inhibitor in the first step of aggregation in $scCO_2$ flooding.

1. Introduction

CO_2 flooding is one of the successful methods for enhanced oil recovery (EOR) applied in oil fields.[1,2] The main mechanisms contributing to oil recovery by CO_2 are the decrease in viscosity and interfacial tension and the increase in mobility of crude oil in oil reservoirs.[3,4] Moreover, supercritical CO_2 ($scCO_2$) has been revealed to be useful for oil extraction due to its properties of low viscosity and high diffusivity.[5] Rudyk *et al.* achieved a total oil recovery ranging from 44–77% when $scCO_2$ was injected into dead oil with a density of 0.8573 kg L^{-1}.[6] However, one of the major drawbacks of CO_2 injection in oil fields is associated with the well-documented asphaltene deposition. This may cause pore throat plugging, permeability reduction, and wettability alteration in reservoirs, further resulting in a reduction in the recovery factor.[7] In addition, deposited asphaltenes can also lead to severe plugging of the wellbore, tubing, and pumps, which must be remediated by constant washing and scrapping.[8] Consequently, this will generate a considerable increase in maintenance costs in the petroleum industry. Therefore, it is important to investigate asphaltene aggregation in the presence of $scCO_2$ to understand the asphaltene aggregation mechanisms and find solutions to the relevant problems.

Asphaltenes, the heaviest and most complicated components in crude oil, consist of polyaromatic species with alkyl side chains and some traces of heteroatoms. Asphaltene molecules tend to aggregate and form larger agglomerates, which is correlated with their molecular structure.[9] According to the recognized Yenn–Mullins model,[10] the aggregation of asphaltenes is a complex hierarchical process. Moreover, asphaltene aggregation is related to the pressure, temperature, and composition of the crude oil. With respect to CO_2-EOR, there have been increasing efforts to study the aggregation behavior of asphaltenes induced by CO_2. Verdier *et al.*[11] investigated the phase behavior of asphaltenes after CO_2 injection into two dead crude oil samples using a high-pressure cell. They observed that the asphaltenes were more stable at high pressure and low temperature. Gonzalez *et al.*[12] investigated the asphaltene phase behavior in a live reservoir fluid and a dead oil, and they found that the perturbed chain-statistical associating fluid theory equation of state model can explicitly account for the effects of CO_2 on asphaltene aggregation behavior. Zanganeh *et al.*[13,14] studied the effects of temperature and pressure on asphaltene deposition during CO_2 injection processes *via* high-pressure cell and image processing techniques. They observed that the amount of deposited asphaltene decreases with a decrease in pressure and temperature has a prominent impact on the size of asphaltene particles. Behbahani and Ghotbi[15] investigated asphaltene aggregation and adsorption using a sandstone core sample during miscible CO_2 injection. They reported that the asphaltenes are adsorbed as a multilayer, with formation of large clusters.

In recent years, numerous efforts have been made to understand asphaltene aggregation at the molecular level using molecular simulations. Using molecular mechanics methods, Murgich *et al.*[16] confirmed that asphaltene aggregation occurs

College of Science, China University of Petroleum, 266580 Qingdao, People's Republic of China. E-mail: liubing19720115@gmail.com; zhangjun.upc@gmail.com

† Electronic supplementary information (ESI) available. See DOI: 10.1039/c7ra09736k

because of stacking of aromatic rings. Rogel[17] studied the interactions of asphaltene aggregates under vacuum and in different solvents. He reported that the stabilization energy is more favorable for molecules with a lower hydrogen-to-carbon ratio, higher aromaticity, and higher aromatic condensation degree. From molecular dynamics simulations, Headen *et al.*[18] reported that asphaltene nanoaggregation occurs in toluene and heptane. They observed that asphaltenes have a stronger tendency to aggregate in $scCO_2$ than in heptane and toluene.[19] Goual *et al.*[20] studied asphaltene aggregation under vacuum, and in toluene and heptane by using an umbrella sampling method to calculate the free energies of asphaltene dimerization. They revealed the important effect of the size of the polynuclear aromatic core, the length of the aliphatic side chains, and heteroatoms on the asphaltene interaction. Furthermore, using molecular dynamics simulations, Headen and Goual[19,21] investigated the prevention of asphaltene deposition in $scCO_2$ by inhibitors. They put forward suggestions for inhibitor selection to limit asphaltene aggregation in $scCO_2$ injection processes. In fact, crude oil is a complex mixture that consists of different hydrocarbons, such as saturated hydrocarbons, aromatics, resins, and asphaltenes (SARA). When the injected $scCO_2$ comes into contact with the crude oil, it leads to the modification of the equilibrium conditions and components of the crude oil. This modification is mainly caused by the intermolecular interactions in oil–$scCO_2$ systems, favoring asphaltene precipitation. Hence, understanding the intermolecular interactions in the system is fundamental to unveiling the mechanism of asphaltene precipitation, which in the CO_2 flooding process is still subject to debate.

In this work, molecular dynamics simulations were performed on an oil–$scCO_2$ system to address primarily the mechanism of asphaltene aggregation upon $scCO_2$ injection in crude oil with SARA. Firstly, the structure of the crude oil was examined in the absence of $scCO_2$. Then 2-D density maps and the radius of gyration were calculated to examine structural variations of the oil components in the presence of $scCO_2$. Finally, the non-bond interaction energy and the potential of mean force (PMF) profile of the molecules were calculated to reveal the mechanism of asphaltene aggregation induced by $scCO_2$.

2. Simulation method

All of the molecular dynamics simulations were performed in the GROMACS 4.5.5 software package.[22] VMD software[23] was used to visualize the results. The CHARMM-27 force field (FF)[24] was used for the oil molecules, which is one of the popular FFs and can reproduce the results in good agreement with experiments for oil molecules.[25–27] CHARMM FF parameters for oil molecules were generated in Swissparam software.[28] The classical three-site EPM2 model[29] was employed to describe carbon dioxide molecules. The long-range electrostatic interactions were treated with the particle mesh Ewald (PME) method.[30] The non-bonded potential truncation was performed with a cut-off radius of 1.0 nm for the Lennard-Jones potential.[31] The temperature was controlled by the Nose–Hoover thermostat algorithm with a coupling constant of 0.2 ps.[32,33] The pressure was controlled by the Parrinello–Rahman algorithm. All simulations were carried out at a temperature of 323.15 K and a pressure of 15 MPa, which are reasonable reservoir conditions and can keep CO_2 in the supercritical state. The initial atomic velocities of the systems were set by the commonly used Maxwell–Boltzmann distribution. The time step was set to 1 fs for all the simulations. Periodic boundary conditions were employed in all three directions.

2.1 Model molecules

According to differences of polarity and molecular weight, the crude oil is separated into SARA, which is a standard analysis method for crude oil composition.[34,35] Although asphaltenes do not have a specific chemical formula, simplification is still feasible to study the main characteristics of asphaltenes. There is a consensus that a single, well-defined compound can model the asphaltene aggregation process successfully.[36] In order to build a more realistic model of crude oil, a widely used continental-type model of asphaltenes ($C_{54}H_{65}NO_2S$, MW: 792)[37] from Venezuelan crude oil was chosen. The chemical structure and the molecular weight of the model are similar to those of asphaltenes in crude oil.[38] The model of the resins ($C_{48}H_{76}S$, MW: 685)[16] was also taken from the spectroscopic data of Venezuelan crude oil. Resins contain less aromatic nuclei and heteroatoms than asphaltenes. Benzoapyrene ($C_{20}H_{12}$, MW: 252) and dodecane ($C_{12}H_{26}$, MW: 170) represented the aromatic and saturate fractions of the crude oil, respectively. The molecular numbers of SARA were established on the basis of the mass ratio of 15 : 30 : 35 : 20, referring to a real heavy crude oil sample.[39,40] From the colloidal instability index (CII), asphaltene stability is mathematically expressed as the sum of asphaltenes and saturates divided by the sum of aromatics and resins.[41] In this work, CII is equal to 0.54, meaning that asphaltenes are quite stable in the crude oil.[42] The molecular configurations are shown in Fig. 1.

2.2 Crude oil system

In order to obtain a proper molecular structure of crude oil, 8 asphaltenes, 18 resins, 60 aromatics and 50 saturates were put

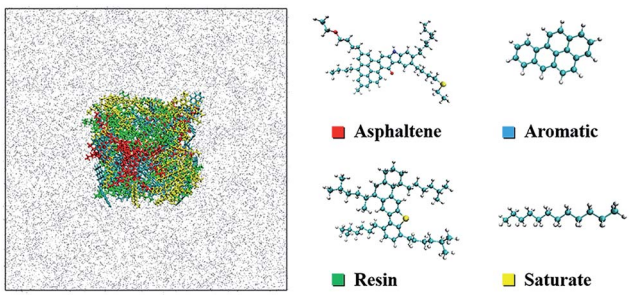

Fig. 1 Sectional view of the simulation setup for the oil–$scCO_2$ system (left) and the molecular structure of SARA components (right). Color scheme: cyan, carbon; white, hydrogen; red, oxygen; yellow, sulfur; blue, nitrogen; grey, CO_2.

into a box randomly using the smart software package Packmol.[43] The steepest descent method was applied for energy minimization. Then a 5 ns MD simulation was performed in the NVT ensemble. After that, a 5 ns MD simulation in the NPT ensemble was performed to represent the equilibrium process of the system and obtain a reasonable volume. Finally, an additional 5 ns MD simulation in the NVT ensemble was performed to collect data for the structural analysis of the crude oil.

2.3 Crude oil–scCO$_2$ system

Firstly, a bulk scCO$_2$ box was built, which was kept in equilibrium by MD simulation in the NPT ensemble. Then, a volume the same size as the oil box was dug out in the center of the scCO$_2$ box. After that, the oil box was placed in the hole. The size of the box is 12 × 12 × 12 nm^3 containing 16 970 scCO$_2$ molecules. A 5 ns MD simulation in the NVT ensemble was performed, in which oil molecules were fixed. Next, the oil molecules were unfixed and a 20 ns MD simulation was performed on the crude oil–scCO$_2$ system in the NVT ensemble.

2.4 Umbrella sampling

PMF is a valid parameter investigating the effective interaction between two molecules. The umbrella sampling method[44] was used to compute the PMF along a given reaction coordinate. Through a series of umbrella sampling simulations, the binding energy between two molecules can be obtained from the PMF. To compute the PMF profile of the target molecules (asphaltene–asphaltene/asphaltene–resin/asphaltene–aromatic) *versus* the center-of-mass (COM) distance, three new simulation boxes including two target molecules were built and then energy minimization, MD simulation in the NPT ensemble, and MD simulation in the NVT ensemble were performed in sequence. The COM of one target molecule was pulled along the *Z*-axis while the other one was restrained. A series of frames were extracted from the trajectory. Each configuration corresponds to the desired COM spacing of less than 0.3 Å. Each of the separate simulations were run along the reaction coordinate ξ, biased by umbrella potentials $w_i(\xi)$. The umbrella potential is expressed as eqn (1):

$$w_i(\xi) = \frac{K_i}{2}(\xi - \xi_i^c)^2 \quad (1)$$

where ξ_i^c is the location at which the system is restrained with a force constant K_i.

For each starting configuration of the sampling window, the data were collected for 5 ns in every sampling window. Three groups of target molecules were placed in scCO$_2$ to perform the sampling simulation procedures again. The PMF profiles were obtained using the Weighted Histogram Analysis Method (WHAM).[45,46]

3. Results and discussion

3.1 Structure of the crude oil in the absence of scCO$_2$

In order to show the effect of scCO$_2$ on asphaltene aggregation, firstly, the structure of the crude oil was studied. When the crude oil system was in equilibrium, the calculated density of the oil was 0.95 g cm^{-3}, coincident with that of actual heavy crude oil under reservoir conditions.[47,48] The configuration of the crude oil is shown in Fig. 2. It shows that the resin molecules tend to aggregate with the asphaltene molecules, rather than coating the asphaltene nanoaggregates, leading to mixed asphaltene–resin aggregates. This result is in line with results from molecular thermodynamics[49] and experiments.[50] Aromatic molecules are distributed closer to the central area of the crude oil compared with the saturates. The saturates tend to be dispersed in the outer region of the heavy components. It should be noted that no parallel stacking configuration of asphaltenes occurs in the crude oil. This may result from the

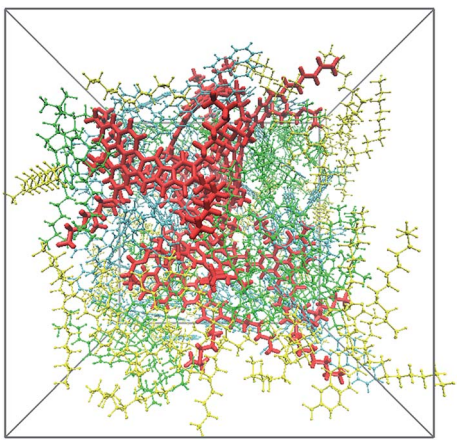

Fig. 2 Perspective view of the crude oil system. Color scheme: red, asphaltenes; green, resins; blue, aromatics; yellow, saturates.

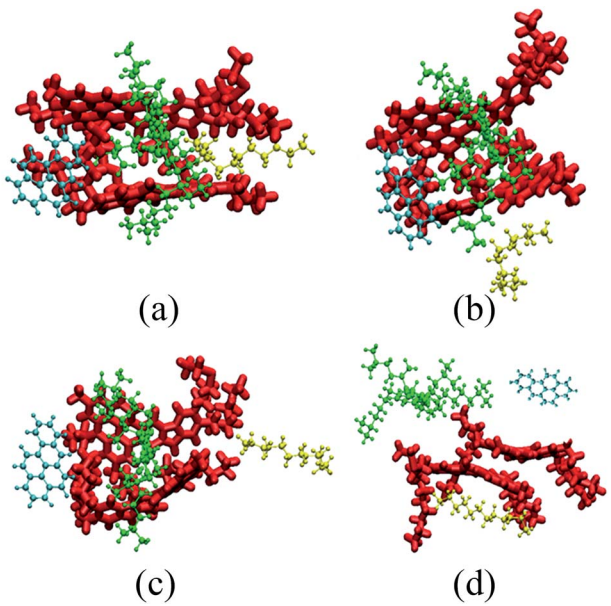

Fig. 3 Representative snapshots of five typical molecules. Snapshots are taken at (a) 0 ns, (b) 1.2 ns, (c) 3.5 ns and (d) 10 ns. The color scheme used in the snapshots is the same as that used in Fig. 2. For clarity, scCO$_2$ is not shown.

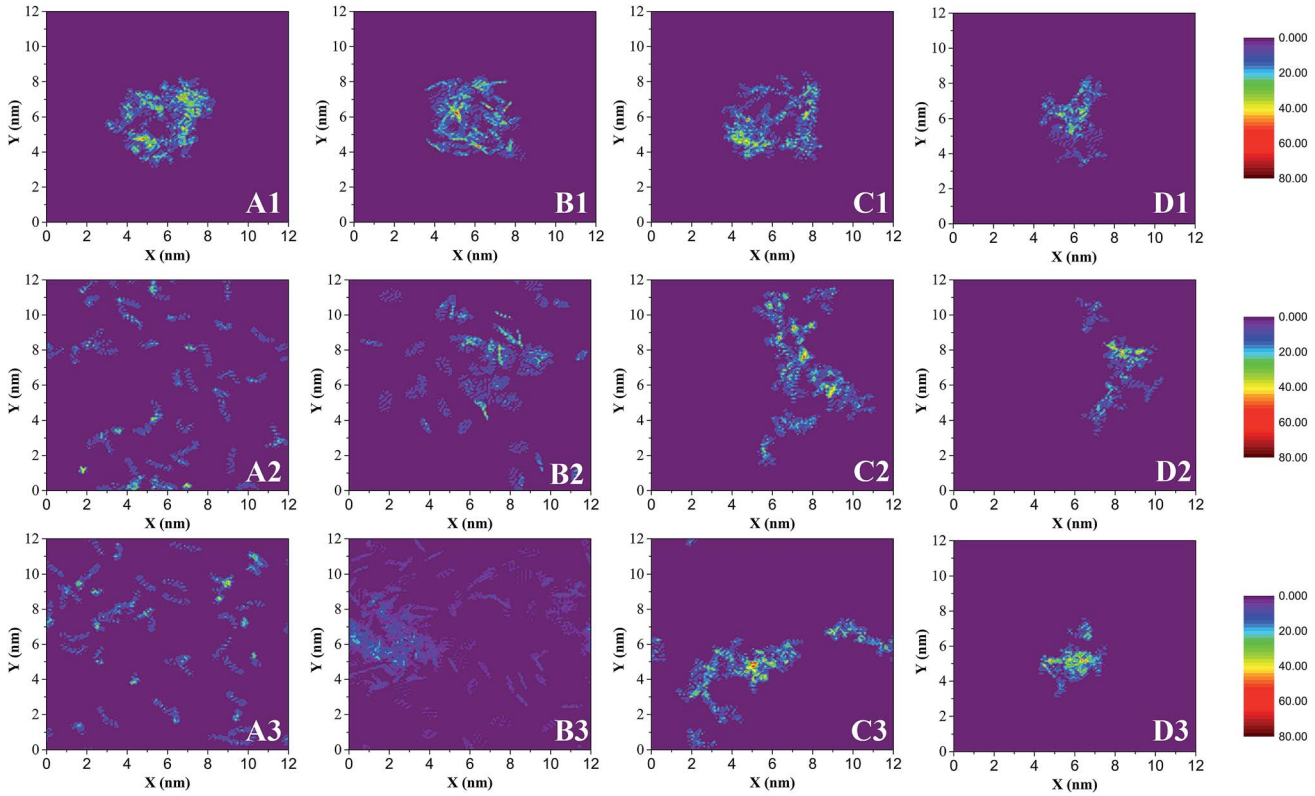

Fig. 4 Planar density distribution of SARA. *Z* is the direction perpendicular to the surface, and the densities are expressed in number of atoms/molecules nm^{-3}. (A) Saturates, (B) aromatics, (C) resins, and (D) asphaltenes. (1), (2) and (3) are taken at 0 ns, 3 ns and 20 ns, respectively.

steric effect of the resin and aromatic molecules. Next, we will investigate the structure of the crude oil in the presence of $scCO_2$.

3.2 Structure of the crude oil in the presence of $scCO_2$

3.2.1 Asphaltene aggregation. To visualize the effect of $scCO_2$ on asphaltene aggregation, we reported the structural alteration of five representative molecules of the crude oil in the presence of $scCO_2$ at different times. The configurations are shown in Fig. 3. It can be seen that upon $scCO_2$ injection into the crude oil, the structure or the distribution of the oil is changed. In addition, a series of snapshots are presented in Fig. S1 of the ESI,† describing the evolution of the oil structure in $scCO_2$. Fig. 3(a) shows that a few of the resins, aromatics and saturates are sandwiched in between two asphaltenes; however, only the side-chains of the resins insert between the asphaltenes. Fig. 3(b) shows that the saturates are first extracted by $scCO_2$, due to like-dissolving-like. Moreover, the strong diffusibility of CO_2 also improves the mutual dissolution between $scCO_2$ and saturates.[51] Fig. 3(c) shows that the aromatic molecules are extracted by the $scCO_2$ later than the saturate molecules, due to the π–π packing interaction. Fig. 3(d) shows that the resins are extracted last. It is also observed that two asphaltenes form a dimer with a parallel structure after the saturates, aromatics, and resins are extracted by $scCO_2$. The COM distance between asphaltenes in the dimer is 3.9 Å, corresponding to the interaction distance between asphaltenes. The dimer structure is maintained to the end. To demonstrate that system equilibrium has been attained, the system's potential energy and the temperature of system are reported in Fig. S2.†

Fig. 3 also shows the significant selective extraction of $scCO_2$ in relation to EOR in the CO_2 flooding process.[52] The order of this extraction is saturate > aromatic > resin, due to the differences in molecular weight and polarity. This can also be described by the diffusibility of SARA in $scCO_2$; the diffusion coefficients of SARA in $scCO_2$ are equal to 9.4462, 3.5748, 2.1838, and 1.4199 (10^{-9} m^2 s^{-1}) respectively. The order of the diffusion coefficients of SARA is saturate > aromatic > resin, indicating that $scCO_2$ has the strongest ability to dissolve saturates, *i.e.* the highest extracting power.

3.2.2 Molecular number density maps of crude oil. To identify the selective extraction of SARA by $scCO_2$, 2-D molecular number density maps of SARA at 0, 3, and 20 ns are reported in Fig. 4. The in-plane number density distributions were obtained along the *Z*-direction and with a grid size of 0.1 nm. Panels A1, A2 and A3 show the number density distributions of saturates in $scCO_2$. It is observed that the saturate distribution changes from the original compactness to the final uniform dispersion in $scCO_2$. This suggests that saturates are easy to extract into $scCO_2$. Panels B1, B2, and B3 describe the number density distributions of aromatics in $scCO_2$. Most of the aromatic molecules are separated and dispersed in $scCO_2$ and only a few of them still accumulate together. However, a less homogeneous dispersion of aromatics than of saturates is observed to be induced by $scCO_2$.

This indicates that $scCO_2$ cannot extract all aromatics from the crude oil, due to the interactions between the aromatics and the heavy components (resins and asphaltenes). Panels C1, C2, and C3 depict the number density distributions of resins in $scCO_2$. It is observed that resins are somewhat dispersed but mainly accumulate together. This implies that $scCO_2$ cannot overcome the interactions between resins and the interactions exerted on resins by asphaltenes. Hence, it is difficult for $scCO_2$ to extract resins from the crude oil and the resins have a strong tendency to gather together. In addition, comparing panel C3 with panel D3, we found an overlap of the densities for resins and asphaltenes, which appears as the brightest color. This indicates that resins tend to be dragged by the asphaltenes, such that they aggregate together with the asphaltenes. Panels D1, D2, and D3 show the number density distributions of asphaltenes in $scCO_2$. We observed that the density distributions of asphaltenes undergo a process whereby they first disperse (panel D2) and then accumulate together (panel D3). In panel D3, the brightest color and the narrowest distribution scope indicate the formation of asphaltene aggregates that are more compact than in their original state. This result is in agreement with experiments.[13,14,53,54] To supply information regarding the *Z*-direction, the radial distribution functions between oil components and CO_2 from further quantitative testing are reported in Fig. S3.†

3.2.3 Radius of gyration of asphaltene aggregates. To quantitatively clarify the process of asphaltene aggregation in $scCO_2$, the radius of gyration (R_g) of the asphaltene aggregates was calculated. R_g describes the mass distribution of asphaltenes forming an aggregate relative to the COM of the aggregate, which is expressed as eqn (2):[55]

$$R_g^2 = \frac{\sum_i m_i (r_i - r_0)^2}{\sum_i m_i} \quad (2)$$

where m_i is the mass of atom i located at the radial distance r_i from the COM of the aggregate.

Fig. 5 shows the R_g of asphaltene aggregates as a function of time. In less than 7 ns, R_g increases quickly, indicating the rapid separation of asphaltene molecules due to the selective extraction of oil components by $scCO_2$. At about 7 ns, an obvious R_g peak occurs, showing that asphaltenes are dispersed in $scCO_2$ to the maximum degree. From 7 ns to 10 ns, R_g decreases steeply, implying the rapid association of the asphaltene molecules. At greater than 10 ns, R_g is essentially unchanged, indicating the stabilization of the asphaltene aggregates. The results are in agreement with the description in Fig. 4(D1–D3). This can be visualized by representative configurations of the contact surface between asphaltenes and $scCO_2$, as shown in Fig. 5. With the extraction of saturates, aromatics, and resins into $scCO_2$, more and more $scCO_2$ occupies the accessible space between asphaltenes. This leads to increasing separation between asphaltenes and a subsequent increase in the contact area between asphaltenes and $scCO_2$, as described by the configuration at 7 ns in Fig. 5. This result indicates that the selective extraction of oil components by $scCO_2$ causes the asphaltenes to be dispersed first, rather than immediately aggregating to form clusters. After most of the components except for the asphaltenes in the crude oil are extracted into $scCO_2$, the asphaltenes begin to associate and form dense nanoaggregates. This can be described by the configuration at 20 ns in Fig. 5. In this work, the diameter of the nanoaggregates is about 2 nm, with an aggregation number of 8, corresponding to the definition of a nanoaggregate in the Yen–Mullins model.[10] We repeated the simulations with different asphaltene molecules and observed the same phenomenon.

From the above analysis of the density distributions and R_g, a two-step process of asphaltene aggregation occurs when $scCO_2$ is injected into crude oil. Asphaltenes experience a process of dispersion as the $scCO_2$ selectively extracts the oil components. After the end of the extraction, the asphaltenes begin to associate with each other and form compact nanoaggregates. This finding demonstrates that the efficiency of inhibiting or mitigating asphaltene aggregation in $scCO_2$ flooding can be significantly improved by controlling the process of selective extraction of oil components by $scCO_2$. Moreover, the time of adding an inhibitor or dispersant into the oil–$scCO_2$ system also influences the inhibition effect.

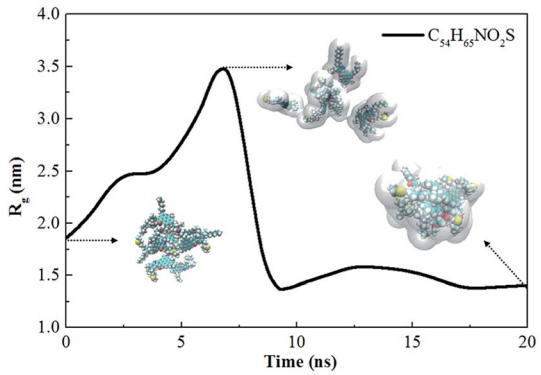

Fig. 5 The time evolution of the gyration radius during a 20 ns simulation. The inset snapshots of asphaltene are taken at 0 ns, 7 ns and 20 ns. The color scheme used in the snapshots is the same as that used in Fig. 1, and the translucent silver surface is the contact surface between asphaltene and CO_2.

Table 1 van der Waals energies, coulomb energies and total interaction energies between asphaltenes

Interaction energies for asphaltene–asphaltene	van der Waals energy (kcal mol^{-1})	Coulomb energy (kcal mol^{-1})	Total (kcal mol^{-1})
Without $scCO_2$	-154.54 ± 1.65	29.91 ± 0.52	-124.63 ± 2.17
With $scCO_2$	-173.66 ± 6.17	25.57 + 2.15	-148.09 ± 8.32

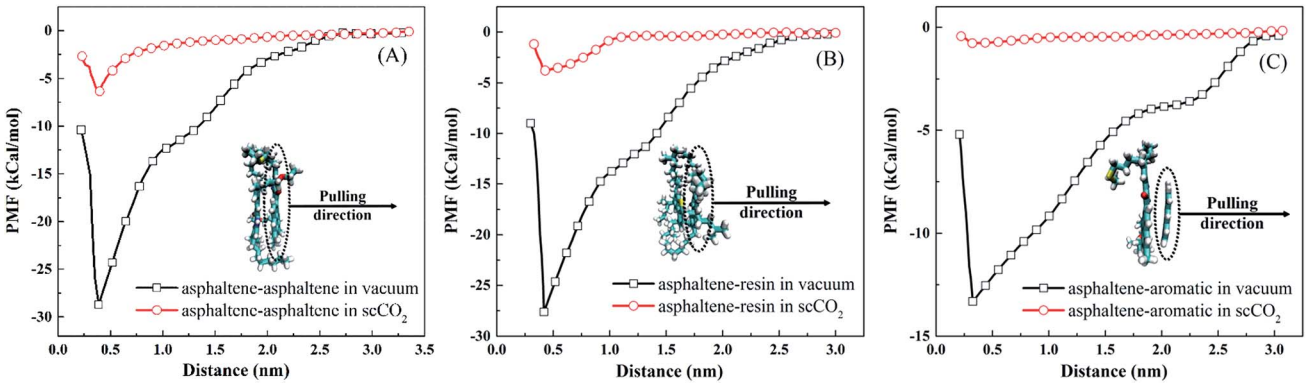

Fig. 6 Potential of mean force profiles for (A) asphaltene–asphaltene, (B) asphaltene–resin, and (C) asphaltene–aromatic, under vacuum and in $scCO_2$. The inset snapshots are the minimum energy state structures, and the color scheme used in the snapshots is the same as that used in Fig. 1.

3.3 The mechanism of asphaltene aggregation

3.3.1 Non-bond interaction energy. Investigating the non-bonding interactions between oil components can help to understand their microcosmic behavior. In this study, intermolecular pair interactions, excluding non-bonded interactions, occur between atoms that are no further than 3 bonds away. The last 3 ns of the simulation in equilibrium were used for computation. The interaction energy among asphaltenes in crude oil and $scCO_2$ is reported in Table 1. The larger the negative value, the stronger the interaction among asphaltenes. It is observed that van der Waals (vdW) interaction and electrostatic interaction both have an effect on the intermolecular interactions of asphaltene. However, vdW interaction plays a predominant role in asphaltene aggregation, whether in the presence of $scCO_2$ or not. The negative total energy implies the tendency to aggregate for asphaltenes. Compared with the total energy in the absence of $scCO_2$, the absolute value of the total energy in the presence of $scCO_2$ is larger. This means that $scCO_2$ injection into the crude oil enhances the aggregation of asphaltenes mainly through improving vdW interactions. In contrast, the interaction energy between asphaltenes and resins drops to -105.32 kcal mol^{-1} from -223.75 kcal mol^{-1}, the interaction energy between asphaltenes and aromatics drops to -206.32 kcal mol^{-1} from -412.41 kcal mol^{-1}, and the interaction energy between asphaltenes and saturates drops to -8.83 kcal mol^{-1} from -109.94 kcal mol^{-1}. The estimated error is within 5.6%.

3.3.2 Potential of mean force. To further explore the effect of $scCO_2$ on asphaltene aggregation, PMFs for asphaltene–asphaltene, asphaltene–resin and asphaltene–aromatic were calculated under vacuum and in $scCO_2$. The results are shown in Fig. 6. The corresponding binding energies for Fig. 6 are presented in Table 2. The binding energy is the difference between the minimum value and the plateau region in the PMF curve. It represents the strength with which two molecules associate with each other. Because asphaltenes are insoluble in saturates,[56] the PMF of asphaltene–saturate was not calculated.

In Fig. 6(A), the asphaltene dimer with the lowest energy shows a diagonal structure. In this structure, the same heteroatoms are in opposite corners at the maximum distance away from each other. This is in agreement with the results obtained by recent quantum mechanical calculations.[57] A shoulder occurs at about 0.9 nm for the PMF curve under vacuum, corresponding to the offset structure of the asphaltene dimer.[20] The PMF reaches a steady value in $scCO_2$ as the separation between them is about 0.6 nm. This indicates that asphaltene aggregates can be stably present in $scCO_2$ as the separation of two asphaltene molecules is less than 0.6 nm. In Table 2, the asphaltene–asphaltene binding energy is -28.82 kcal mol^{-1} under vacuum. This value is slightly lower than that obtained by quantum mechanical calculations[58] and higher than that from atomistic calculations.[59] The difference may come from the difference in the asphaltene model used in these studies. π–π interaction is believed to be the driving force to form the face-to-face stacked structure, which was confirmed by recent studies.[60,61] The binding energy of asphaltene–asphaltene in $scCO_2$ drops to -6.9 kcal mol^{-1}, which is much lower than that under vacuum. This indicates that asphaltenes are less prone to aggregation in $scCO_2$ than under vacuum. The remaining strength of association between asphaltene molecules is the reason why the asphaltene aggregates are stable in $scCO_2$, as shown in Fig. 4(D3) and Fig. 5.

Table 2 The binding energies between asphaltene–asphaltene, asphaltene–resin, and asphaltene–aromatic

Binding energy (kcal mol^{-1})	Asphaltene–asphaltene	Asphaltene–resin	Asphaltene–aromatic
Under vacuum	-28.82 ± 0.65	-27.61 ± 0.62	-13.94 ± 0.47
In $scCO_2$	-6.90 ± 0.42	-3.82 ± 0.38	-0.51 ± 0.09

In Fig. 6(B), the PMF profile of asphaltene–resin is similar to that of asphaltene–asphaltene under vacuum. The binding energy between asphaltenes and resins is −27.61 kcal mol^{-1}, which is very close to that between two asphaltenes, as shown in Table 2. This indicates that resins tend to associate with asphaltenes and form mixed asphaltene–resin aggregates in crude oil. In $scCO_2$, the binding energy between asphaltenes and resins drops to −3.82 kcal mol^{-1}. This indicates that it is hard for the mixed asphaltene–resin aggregates to survive in $scCO_2$. However, this nonzero binding energy implies that the resin molecules can be dragged together by asphaltenes. This can be observed in Fig. 3 and 4(C3).

In Table 2, the binding energy of asphaltene–aromatic under vacuum is −13.94 kcal mol^{-1}, significantly lower than that of either asphaltene–asphaltene or asphaltene–resin. Thus, compared with the resins, the aromatics are more distant from the asphaltenes in crude oil. The binding energy between asphaltenes and aromatics is −0.51 kcal mol^{-1} in $scCO_2$. This indicates that $scCO_2$ can significantly reduce the effective interaction between asphaltenes and aromatics. Consequently, aromatics can be more easily extracted from the crude oil by $scCO_2$ than resins.

It can be concluded that the order of the binding energy is asphaltene–asphaltene > asphaltene–resin > asphaltene–aromatic, both under vacuum and in $scCO_2$. The ratio of the binding energies for asphaltene–asphaltene, asphaltene–resin and asphaltene–aromatic changes from 1 : 0.96 : 0.48 under vacuum to 1 : 0.55 : 0.07 in $scCO_2$. The results also indicate that $scCO_2$ can easily destroy the associations of asphaltene–resin and asphaltene–aromatic, which promotes asphaltene aggregation. From the above analysis, we can conclude that asphaltene aggregation in $scCO_2$ results from the synergistic effect of selective extraction of oil components and the remaining strength of association between asphaltenes.

4. Conclusion

In this study, MD simulations were performed to investigate the dynamic process and microscopic mechanism of asphaltene aggregation in $scCO_2$. The results show that resins tend to associate with asphaltenes in the absence of $scCO_2$, and asphaltenes cannot form compact aggregates because of the steric effect of the resin and aromatic molecules. In the presence of $scCO_2$, the order of selective extraction is saturate > aromatic > resin. This leads to asphaltenes accumulating and forming compact nanoaggregates in $scCO_2$. In the process of asphaltene aggregation, asphaltenes firstly separate from each other, due to the extraction behavior of $scCO_2$. After the separation stage, the asphaltenes associate with each other to form nanoaggregates that stably exist in $scCO_2$.

The aggregation mechanism was investigated from the point of view of energy, and it was observed that vdW interaction plays a predominant role in asphaltene aggregation, both in the absence and presence of $scCO_2$. Furthermore, the coulomb interaction energy decreases and the vdW interaction energy increases due to the presence of $scCO_2$, which aggravates asphaltene aggregation. The free energy calculations show that the binding energy of asphaltene–asphaltene is close to that of asphaltene–resin under vacuum, which implies that resins tend to mix with asphaltenes in crude oil. In $scCO_2$, the binding energies of asphaltene–resin and asphaltene–aromatic were significantly decreased. Meanwhile the remaining −6.9 kcal mol^{-1} binding energy of asphaltene–asphaltene in $scCO_2$ is responsible for the existence of asphaltene aggregates.

The dynamic process and microscopic mechanism are helpful in providing some useful information for guiding $scCO_2$-enhanced oil recovery, especially for predicting and avoiding asphaltene aggregation. However, research on asphaltene inhibition is still inadequate, and our future work will focus on effective approaches to asphaltene inhibition.

Conflicts of interest

The authors declare no competing financial interest.

Acknowledgements

This work was financially supported by the PetroChina Innovation Foundation (2017D-5007-0206), the National Basic Research Program of China (2014CB239204), and the Fundamental Research Funds for the Central Universities (15CX08003A).

References

1 F. Gozalpour, S. R. Ren, B. Tohidi and F. Gozalpour, *Oil Gas Sci. Technol.*, 2005, **60**, 537–546.
2 E. Tzimas, A. Georgakaki, C. G. Cortes and S. D. Peteves, *Report EUR 21895 EN*, European Commission, 2005.
3 R. Farajzadeh, A. Andrianov, H. Bruining and P. L. J. Zitha, *Ind. Eng. Chem. Res.*, 2009, **48**, 4542–4552.
4 M. L. Godec, V. A. Kuuskraa and P. Dipietro, *Energy Fuels*, 2013, **27**, 4183–4189.
5 R. G. Santos, W. Loh, A. C. Bannwart and O. V. Trevisan, *Braz. J. Chem. Eng.*, 2014, **31**, 571–590.
6 S. Rudyk, S. Hussain and P. Spirov, *J. Supercrit. Fluids*, 2013, **78**, 63–69.
7 R. Nguele, M. R. Ghulami, K. Sasaki, H. Said-Al Salim, A. Widiatmojo, Y. Sugai and M. Nakano, *Energy Fuels*, 2016, **30**, 1266–1278.
8 B. Ju, T. Fan and Z. Jiang, *J. Pet. Sci. Eng.*, 2013, **109**, 144–154.
9 I. David Borton, D. S. Pinkston, M. R. Hurt, X. Tan, K. Azyat, A. Scherer, R. Tykwinski, M. Gray, K. Qian and H. I. Kenttämaa, *Energy Fuels*, 2015, **24**, 5548–5559.
10 O. C. Mullins, H. Sabbah, J. Eyssautier, A. E. Pomerantz, L. Barré, A. B. Andrews, Y. Ruizmorales, F. Mostowfi, R. Mcfarlane and L. Goual, *Energy Fuels*, 2012, **26**, 3986–4003.
11 S. Verdier, H. Carrier, S. I. Andersen and J.-L. Daridon, *Energy Fuels*, 2006, **20**, 1584–1590.
12 D. L. Gonzalez, F. M. Vargas, G. J. Hirasaki and W. G. Chapman, *Energy Fuels*, 2008, **22**, 757–762.
13 P. Zanganeh, S. Ayatollahi, A. Alamdari, A. Zolghadr, H. Dashti and S. Kord, *Energy Fuels*, 2012, **26**, 1412–1419.
14 P. Zanganeh, H. Dashti and S. Ayatollahi, *Fuel*, 2015, **160**, 132–139.

15 T. J. Behbahani, C. Ghotbi, V. Taghikhani and A. Shahrabadi, *Fuel*, 2014, **133**, 63–72.
16 J. Murgich, J. Rodríguez and Y. Aray, *Energy Fuels*, 1996, **10**, 68–76.
17 E. Rogel, *Energy Fuels*, 2000, **14**, 566–574.
18 T. F. Headen, E. S. Boek and N. T. Skipper, *Energy Fuels*, 2009, **23**, 1220–1229.
19 T. F. Headen and E. S. Boek, *Energy Fuels*, 2010, **25**, 503–508.
20 M. Sedghi, L. Goual, W. Welch and J. Kubelka, *J. Phys. Chem. B*, 2013, **117**, 5765.
21 E. Lowry, M. Sedghi and L. Goual, *Energy Fuels*, 2016, **30**, 7187–7195.
22 B. Hess, C. Kutzner, d. S. D. Van and E. Lindahl, *J. Chem. Theory Comput.*, 2008, **4**, 435–447.
23 W. Humphrey, A. Dalke and K. Schulten, *J. Mol. Graphics*, 1996, **14**, 33–38.
24 P. Bjelkmar, P. Larsson, M. A. Cuendet, B. Hess and E. Lindahl, *J. Chem. Theory Comput.*, 2010, **6**, 459–466.
25 W. Xie, H. Liu, Y. Sun, H. Fu and Y. Liang, *Appl. Surf. Sci.*, 2017, **392**, 747–759.
26 Y. Yan, C. Li, Z. Dong, T. Fang, B. Sun and J. Zhang, *Fuel*, 2017, **190**, 253–259.
27 Y. Yu, I. A. Fursule, L. C. Mills, D. L. Englert, B. J. Berron and C. M. Payne, *J. Mol. Graphics Modell.*, 2017, 32–42.
28 V. Zoete, M. A. Cuendet, A. Grosdidier and O. Michielin, *J. Comput. Chem.*, 2011, **32**, 2359.
29 J. G. Harris and K. H. Yung, *J. Phys. Chem.*, 1995, **99**, 12021–12024.
30 T. Darden, D. York and L. Pedersen, *J. Chem. Phys.*, 1993, **98**, 10089–10092.
31 L. Verlet, *Phys. Rev.*, 1967, **159**, 98.
32 D. J. Evans and B. L. Holian, *J. Chem. Phys.*, 1985, **83**, 4069–4074.
33 G. J. Martyna, M. L. Klein and M. Tuckerman, *J. Chem. Phys.*, 1992, **97**, 2635–2643.
34 K. A. Bissada, J. Tan, E. Szymczyk, M. Darnell, M. Mei and J. Zhou, *Org. Geochem.*, 2016, **95**, 21–28.
35 N. Aske, H. Kallevik and J. Sjöblom, *Energy Fuels*, 2001, **15**, 1304–1312.
36 B. Breure, D. Subramanian, J. Leys, C. J. Peters and M. A. Anisimov, *Energy Fuels*, 2012, **27**, 172–176.
37 E. Rogel, *Colloids Surf., A*, 1995, **104**, 85–93.
38 O. C. Mullins, B. Martínez-Haya and A. G. Marshall, *Energy Fuels*, 2008, **22**, 1765–1773.
39 P. Liu, Q. Shi, K. H. Chung, Y. Zhang, N. Pan, S. Zhao and C. Xu, *Energy Fuels*, 2010, **24**, 5089–5096.
40 S. Ashoori, M. Sharifi, M. Masoumi and M. M. Salehi, *Egypt. J. Pet.*, 2017, **26**(1), 209–213.
41 I. A. Wiehe and R. J. Kennedy, *Energy Fuels*, 2000, **14**, 56–59.
42 A. P. W. S. Asomaning, *Heat Transfer Eng.*, 2000, **21**, 10–16.
43 L. Martínez, R. Andrade, E. G. Birgin and J. M. Martínez, *J. Comput. Chem.*, 2009, **30**, 2157–2164.
44 J. Kästner, *Wiley Interdiscip. Rev.: Comput. Mol. Sci.*, 2011, **1**, 932–942.
45 S. Kumar, J. M. Rosenberg, D. Bouzida, R. H. Swendsen and P. A. Kollman, *J. Comput. Chem.*, 1992, **13**, 1011–1021.
46 J. S. Hub, B. L. De Groot and D. Van Der Spoel, *J. Chem. Theory Comput.*, 2010, **6**, 3713–3720.
47 S. E. Quiñones-Cisneros, S. I. Andersen and J. Creek, *Energy Fuels*, 2005, **19**, 1314–1318.
48 B. Quail, G. Hill and K. N. Jha, *Ind. Eng. Chem. Res.*, 1988, **27**, 519–523.
49 E. Rogel, *Energy Fuels*, 2008, **22**, 3922–3929.
50 M. Sedghi and L. Goual, *Energy Fuels*, 2010, **24**, 2275–2280.
51 A. T. Grogan, V. W. Pinczewski and G. J. Ruskauff, *SPE Reservoir Eng.*, 1988, **3**, 93–102.
52 T. Fang, J. Shi, X. Sun, Y. Shen, Y. Yan, J. Zhang and B. Liu, *J. Supercrit. Fluids*, 2015, **113**, 10–15.
53 R. Nguele, M. R. Ghulami, K. Sasaki, S. A. Salim, A. Widiatmojo, Y. Sugai and M. Nakano, *Energy Fuels*, 2016, **30**(2), 1266–1278.
54 A. Alizadeh, H. Nakhli, R. Kharrat, M. H. Ghazanfari and M. Aghajani, *Energy Sources, Part A*, 2014, **36**, 1523–1530.
55 M. K. Shimamura and T. Deguchi, *Phys. Rev. E: Stat., Nonlinear, Soft Matter Phys.*, 2002, **65**, 126.
56 P. Luo, X. Wang and Y. Gu, *Fluid Phase Equilib.*, 2010, **291**, 103–110.
57 M. Mousavi, T. Abdollahi, F. Pahlavan and E. H. Fini, *Fuel*, 2016, **183**, 262–271.
58 A. Ortega-Rodriguez, C. Lira-Galeana, Y. Ruiz-Morales and S. Cruz, *Pet. Sci. Technol.*, 2001, **19**, 245–256.
59 F. Alvarez-Ramirez, E. Ramirez-Jaramillo and Y. Ruiz-Morales, *Energy Fuels*, 2006, **20**, 195–204.
60 H. Wang, H. Xu, W. Jia, J. Liu and S. Ren, *Energy Fuels*, 2017, **31**, 2488–2495.
61 J. Liu, Y. Zhao and S. Ren, *Energy Fuels*, 2015, **29**, 1233–1242.